Accepted Manuscript

Electrochemical characterization of Polypyridine Iron (II) and Cobalt (II) complexes for organic redox flow batteries

Elisabetta Benazzi, Vito Cristino, Stefano Caramori, Laura Meda, Rita Boaretto, Carlo Alberto Bignozzi

Please cite this article as: E. Benazzi, V. Cristino, S. Caramori, L. Meda, R. Boaretto, C.A. Bignozzi, Electrochemical characterization of Polypyridine Iron (II) and Cobalt (II) complexes for organic redox flow batteries, *Polyhedron* (2017), doi: https://doi.org/10.1016/j.poly.2017.12.001

Electrochemical characterization of Polypyridine Iron (II) and Cobalt (II) complexes for organic redox flow batteries

Elisabetta Benazzi*[a], Vito Cristino,[a] Stefano Caramori,[a]* Laura Meda,[b] Rita Boaretto[a] and

Carlo Alberto Bignozzi[a]

[a] *Department of Chemistry and Pharmaceutical Sciences, University of Ferrara, Via Fossato di Mortara 17, 44121 Ferrara, Italy*

[b]*Renewable Energy and Environmental R&D Center, ENI Novara, Italy*

Corresponding Authors E-mail: bnzlbt@unife.it, cte@unife.it.

Abstract

The electrochemical properties of a series of complexes based on chelate ligands were explored with the aim of finding promising candidates for applications in high voltage organic flow cells. The combination of Co(II)/(I) and Fe(III)/(II) as the cathodic and the anodic couple leads to open circuit voltages close to 2 V and to limiting current of the order of 30 mA/cm^2 in 0.3 M concentration in a mixture of Ethylene and Propylene Carbonates. The best solubility was found for bis-cationic complexes as triflate (OTf) salts, reaching > 0.6 M at room temperature. Potentiostatic and potentiodynamic experiments point to a substantial chemical and electrochemical stability at carbon based electrodes as well.

1.Introduction

Redox flow batteries are attractive devices in the framework of the storage of renewable energies in stationary power plants, which could be sized for both domestic and industrial applications ranging from kW to MW size [1]. In these conditions their main limitation, i.e. low energy density, relatively large volume, poor portability are relatively unimportant [2]. Their fundamental operation is relatively straightforward: in the charge phase the current generated by the solar power plant converts two redox couples (or the same redox species with at least two distinct redox states) in their respective oxidized and reduced form, which are stored in separate compartments. In the discharge phase, the battery operates the reverse reaction, i.e. the reduced and oxidized forms are restored to their initial state supplying current to the external load [1]. Among liquid flow-batteries, Vanadium redox flow-batteries are nowadays established prototypes in phase of advanced

development [3-5] having a favorable performance/cost ratio. These are however not immune from concerns and problems, since vanadium batteries operate in strongly acidic media [6] (typically sulfuric acid > 1 M) and vanadium in the V(V) state is a carcinogenic agent. The large scale-up of aqueous batteries is contrasted by their limited energy density, both due to the small potential window (1.23V) for water stability (which essentially coincides with the voltage delivered by the V(V)/V(IV) and V(III)/V(II) redox couples) and by the limited solubility of a variety of couples having promising properties for these applications [7]. More recently, first row transition metal complexes have been considered as redox active species in non-aqueous redox flow batteries (NA-RFB) with encouraging results [8]. Advantages to employ transition complexes as redox couples in NA-RFB are many: the availability of a broader array of redox-active species for new redox couples; the possibility to easily tune their electrochemical properties by varying the coordination sphere of transition complexes; the existence of wider stability windows in non-aqueous solvents; the possibility to reach higher energy density and multiple electron transfer. The Earth-abundant metals, which are available at relatively low cost, comprise chiefly first row transition elements such as Mn [9], Fe [10-13], Co [11-15], Ni [10], Cr [16, 17] and V [18]. In the present state metal-complexes in NA-RFBs do not compete with vanadium RFBs in terms of long-term performance and additional possibilities must be considered [19]. In this study we have explored the electrochemical properties of a series of cobalt (Co(II)/(I)) and iron (Fe(III)/(II)) complexes as triflate and tetrabutyl-ammonium salts, in the effort of coupling solubility and reversible or quasi-reversible electrochemistry to the possibility of extracting large cell voltages (Fig.1).

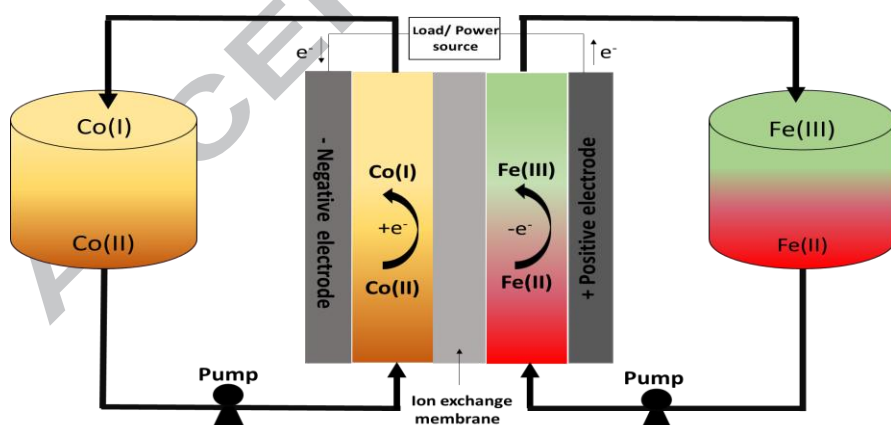**Fig.1**- Schematic of a Co(II)/Co(I) and Fe(III)/Fe(II) based redox flow battery. The cell is shown under charge.

Co(II) to Co (I) reduction and Fe(II) to Fe(III) oxidation are centered on orbitals with prevailing metal character, with low spin configuration favored in the case of strong field ligands [20]. This avoids, unlike cathodic and anodic couples based on organic species, formation of organic radicals

2

characterized by high reactivity, which can give rise to collateral reactions damaging the long-term chemical stability of the cell. Clearly, the redox potential in Iron and Cobalt complexes depends on their coordination sphere, allowing a fine adjustment of potential via synthetic design. In order to find ligands suitable for use in redox flow batteries, it is interesting to note that there is a large synthetic library developed in recent years in the field of dye-sensitized solar cells, where both the chromophore and the redox mediator are often coordination compounds whose redox properties are tuned to optimize harvesting and energy conversion [21]. Oxidative and reductive processes centered on metals do not involve breaking and formation of chemical bonds and are often kinetically fast mono-electronic processes, implying, in principle, reduced overvoltage during device charge and discharge. Synthetic simplicity and chemical stability have oriented us mainly towards the preparation of polypyridine chelants derived by pyridine coupling, i.e. bipyiridines and terpyridines possibly substituted in the 4,4' positions by alkyl-groups. Co(II) or Fe(II) complexes can be generated by mixing appropriate Co(II) or Fe(II) salts with stoichiometric ratios of monodentate, or tridentate ligands, or mixture of these. In particular, our work is focused on the study of Cobalt(II) **1**, **2**, **3** [22], **4** [23], **5** (Fig. 2) species used as cathodic couples and Iron(II) **6, 7,8 ,9** [24] complexes as anodic couples (Fig. 3). 4-4' substituents of 2-2'-bipyridine were considered in order to cathodically shift the redox potential of Co(II)/Co(I) and in general, to tune solubility in the organic solvents. Moreover, a cobalt hexadentate (**5**) and a negatively charged heteroleptic complex (**4**) were synthesized in order to test higher stability with respect to either ligand dissociation or electrode passivation under negative polarization.
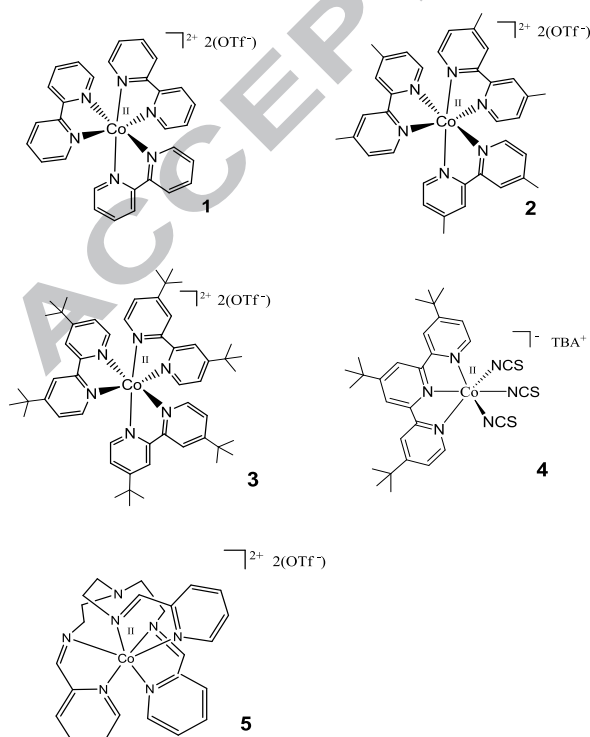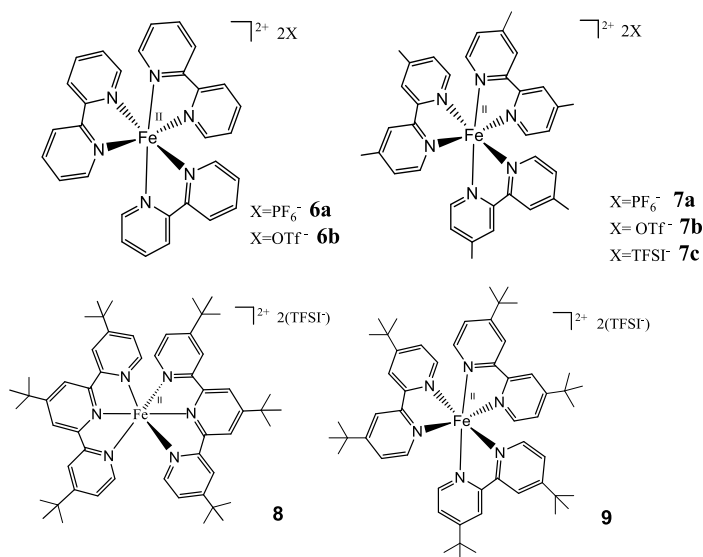
Fig.2– Co(II) complexes chosen for electrochemical testing (where TBA= tetrabutyl-ammonium ion).

Fig.3– Fe(II) complexes chosen for electrochemical testing (where TFSI⁻ = Bis(trifluoromethane)sulfonimide anion)

2. Experimental

2.1. Materials and Methods

All chemicals were Sigma Aldrich products and were used as received: Cobalt(II) carbonate hydrate ($CoCO_3$, ≥97%), triflic acid (HOTf, ≥99%), 2,2'-bipyridine (bpy, ≥99%), 4,4'-dimethyl-2,2'-bipyridine (dmb, 99%), 4,4'-di-*tert*-butyl-2,2'-bipyridine (dtb, 98%), ammonium Iron(II) sulfate hexahydrate (($NH_4)_2Fe(SO_4)_2 \times 6(H_2O)$, 99.9%), 4,4',4''-tri-*tert*-butyl-2,2':6',2''-terpyridine (ttt, 95%), tetrabutylammonium hexafluorophosphate (TBAPF$_6$, ≥99%), nitrosyl tetrafluoroborate (NOBF$_4$, 95%), Sodium hydroxide (NaOH, ≥97%), tetrabutylammonium thiocyanate (TBANCS, 98%), lithium triflate (LiOTf, 99.9%), bis(trifluoromethane)sulfonimide lithium salt (LiTFSI, ≥95%), ammonium cerium(IV) nitrate (CAN, ≥98.5%), 3-4-ethylenedioxythiophene (EDOT, 97%). The following solvents were Sigma-Aldrich and were used as received: Diethyl ether (ACS reagent, ≥99%), Acetonitrile (AcN, for HPLC, gradient grade ≥99.9%), methanol (MeOH, anydrous, 99.8%), Propylene carbonate (PC, reagent grade, 99%), Ethylene carbonate (EC, anhydrous, 99%), Acetone (for HPCL, ≥99.9%), Methanol-d (CD$_3$OD, ≥99.8 atom % D), Acetonitrile-d (CD$_3$CN, ≥99.8 atom % D), Chloroform-d (CD$_3$Cl, ≥99.8 atom % D). The solvent mixtures AcN:PC and

EC:PC were prepared by mixing respectively Acetonitrile and Propylene carbonate (1:1) and Ethylene carbonate and Propylene carbonate (1:1).

NMR spectra were obtained on Bruker Advance III 400 MHz (^{1}H) spectrometer. Chemical shifts (δ) of spectra are expressed in ppm relative to Me$_4$Si. Spectra were processed with MNOVA.

Mass spectrometry was performed in ESI mode with a Finningan LCQ Duo Ion Trap (Capillary Temp: 250 °C, Infusion flow rate: 18 μL/min, Sheath gas flow rate: 20 AU), or with a Waters Micromass ZQ 2000 (Cone Temperature 110°C and desolvation Temperature of 130°C, Capillary voltage 2.30 KV, Cone Voltage 20 V, Extractor Voltage 3V and RF Lens Voltage 0.3V, Flow rate 295 L/hr) under positive/negative mode acquisition.

IR spectroscopy in Diffuse Reflectance mode were collected in KBr powder with a Nicolet Vertex 70 FTIR with a resolution of 4 cm^1.

Electrochemical studies on glassy carbon electrodes (Amel) were carried out by cyclic voltammetry (CV) and by Electrochemical Impedance Spectroscopy (EIS) in a standard three-electrode cell with an Autolab PGSTAT 302/N potentiostat and with a standard calomel electrode as reference (Amel) and a Pt wire as auxiliary (Sigma-Aldrich). Impedance spectra were fitted with Z-View by using the electric equivalent reported in Scheme 1 where R1 is the serial Ohmic resistance (Rs), CPE1 is the constant phase element (non ideal interfacial capacitance), R2 is the charge transfer resistance (Rct) and Wo1 is the open Warburg element.
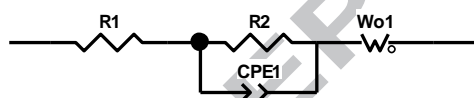
Scheme 1-Equivalent circuit for fitting the EIS data in three-electrode cell.

Electrochemical studies on carbon felts (Sigracell$^@$ GFD4.6 EA) were carried out by Chronoamperometry and by cyclic voltammetry in a standard three-electrode cell with an Autolab PGSTAT 302/N potentiostat and with a standard calomel electrode as reference (Amel) and a Pt wire as auxiliary (Sigma-Aldrich). Cyclic voltammetries were recorded at scan rates varying between 2mV/s and 200mV/s in a EC:PC + 0.1M LiOTf solution with dynamic IR-drop compensation and the redox couple concentration was 10^{-3} M. Apparent heterogeneous electron transfer rate constants (k^0) (Table 3) were obtained by plotting ln(Ip) vs Ep-E$_{1/2}$ as function of the scan rate (Fig.S15 b, Fig.S16 b) (Eq.1) [25] from the fits of the linear trait of the curve. The

5

diffusion coefficients (D) of the Co(II)/Co(I) and Fe(III)/Fe(II) species were calculated from the Randles-Sevcik equation (Fig.S15 a, Fig.S15 a) (Eq.2) after determination of the electroactive area of the felt with a 10^{-3}M ferrocene standard (D = 1.06×10^{-6} cm^{2}s^{-1} in EC:PC).

Eq.1 $\ln(Ip) = \ln(0.227 nFk^0 AC) + (\alpha nF/RT)(Ep - E_{1/2})$

Eq.2 $Ip = (2.99 \times 10^5) \, n^{3/2} \, \alpha^{1/2} \, AD_{red}^{1/2} \, v^{1/2} \, C$

In Eq.1 and Eq.2 n represents the number of exchanged electrons, C the bulk concentration of the electroactive species, Ep and $E_{1/2}$ the peak and the half wave peak potentials respectively, A the electrode surface area, v the scan rate, and D_{red} the diffusion coefficient of the complexes when using anodic peak current.

Absorption spectra were collected with a JASCO V 570 UV–Vis spectrophotometer in 1 cm path quartz cuvettes. Resolution of 1 nm was used.

Oxidation-reduction cycles were carried out in EC:PC + 1M LiOTf on a 10^{-3} M solution of complex **6b** by chronoamperometry in a standard three-electrode cell with an Autolab PGSTAT 302/N potentiostat and with a standard calomel electrode as reference (Amel) and a Pt wire as auxiliary (Sigma-Aldrich), by employing a carbon felt working electrode (Sigracell$^@$ GFD4.6 EA) (1cm^2 Area).

Spectroelectrochemical measurements on Fe(III)/(II) were carried out in EC:PC + 1M LiOTf on a 10^{-3}M solution of complex **6b** in 2 mm path three-electrode quartz cell with an Autolab PGSTAT 302/N potentiostat and a JASCO V 570 UV–Vis spectrophotometer. In order to oxidize **6b,** a potential of 1.5V was applied for 500s and a potential of 0V was applied for 730s to reduce the oxidized species formed in the first potential step. A standard calomel electrode as reference (Amel), a Pt wire as auxiliary (Sigma-Aldrich) and a transparent ITO working electrode (Sigma-Aldrich) (2×0.5cm^2 Area) were employed.

Impedance spectroscopy measurements (EIS) and slow scan rate cyclic voltammetry in symmetric (i.e. two identical electrodes) thin layer cells having active area of 0.25 cm^2 sealed with a 25 μm inter-electrode spacing (Surlyn®, DuPontTM), were carried out with an Autolab PGSTAT 302/N potentiostat, employing two different kind of electrodes to study Fe(III)/(II) and Co(II)/(I) complexes. PEDOT (Poly(3-4-ethylenedioxythiophene) films were electrodeposited [22] on FTO (Pilkington) to study the Fe(III)/Fe(II) couple while carbon nanohorns (CNH) (Carbonium s.r.l) based electrodes were spray deposited [26] on FTO to study Co(II)/Co(I). Contrary to PEDOT, which is insulating at cathodic voltages, nanohorn films present a large electroactivity window,

6

which allows to intercept the Co(II)/Co(I) couple. EIS experiments were carried out at the equilibrium voltage potential (0 V) of Fe(III)/(II) couple and at the half wave potential (ca -1.25 V) of the Co(II)/(I) couple. Impedance spectra were fitted with Z-View by using the electric equivalent reported in Scheme 2 where R1 is the serial Ohmic resistance (Rs), CPE1 is the constant phase element, R2 is the charge transfer resistance (Rct) and Ws1 is the short Warburg element.
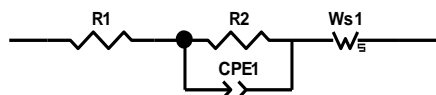
Scheme 2 Equivalent circuit for fitting the EIS data in symmetric thin layer cell.

2.2 Synthesis of [Co(H₂O)₆](OTf)₂

$[Co(H_2O)_6](OTf)_2$ was synthesized by a standard procedure reported in literature [24]: 3 g of $CoCO_3$ were suspended under magnetic stirring in 50 ml of distilled water and HOTf was added dropwise under pH-metric control (the pH was never lowered below 4.5). During the course of the reaction CO_2 evolved and the formation of a transparent pink solution of $[Co(H_2O)_6](OTf)_2$ was observed. The addition of acid ceased when no further evolution of CO_2 was observed. The solution was filtered to remove minor dark insoluble impurities and the solvent was evaporated under reduced pressure. The resulting hygroscopic solid was preserved in a desiccator.

2.3 Synthesis of complexes 1,2,3

Cobalt complexes **1**, **2** and **3** were synthesized according to a literature procedure [22] by mixing 1eq. of $[Co(H_2O)_6](OTf)_2$ salt (1g, 2.8mmol) with 3 eq. of the appropriate ligand (respectively 2,2'-bipyridine (bpy) (1.31g, 8.4mmol), 4,4'-dimethyl-2,2'-bipyridine (dmb) (1.55g, 8.4mmol), 4,4'-di-*tert*-butyl-2,2'-bipyridine (dtb) (2.25g, 8.4mmol) in methanol solution. Solution was stirred for 15 minutes, and the final product was obtained by evaporation under vacuum. All complexes were purified by dissolving the solid in a minimum amount of acetonitrile, followed by precipitation with diethyl ether and drying at room temperature. Yield **1**: 89% (2.06g, 2.5mmol); Yield **2**: 85% (2.16g, 2.38mmol); Yield **3**: 86% (2.8g, 2.4mmol). The diamagnetic oxidized form of the respective complexes (for ^{1}H-NMR characterization) was obtained by addition of a slight excess of $NOBF_4$ in acetonitrile followed by rotary evaporation of the solvent.

^{1}H NMR (400 MHz) CD_3CN ,δ (ppm): $[Co(bpy)_3]^{3+}$: 8.68 (dd, 6H), 8.38 (m, 6H), 7.74 (m, 6H), 7.27 (d, broad, 6H); $[Co(dmb)_3]^{3+}$: 8.65 (d, 6H); 7.92 (dd, 6H); 7.4 (d, 6H); 2.48 (s, 18H); $[Co(dtb)_3]^{3+}$: 8.66 (d, 6H), 7.7 (dd, 6 H), 7.1 (d, 6 H), 1.5 (s, 54 H).

^{1}H-NMR is according to data reported in literature [22]

2.4 Synthesis of complex 4

Complex **4** was obtained by treating 1e.q of [Co(H₂O)₆](OTf)₂ (1g, 2.8mmol) with 1 eq. of 4,4',4''-tri-*tert*-butyl-2,2':6',2''-terpyridine (ttt) (1.24g, 2.0mmol) in acetone and by adding an excess of TBANCS (6eq.) [23](5g, 16.8mmol) that was intentionally left to avoid Co-NCS dissociation in the operational cell. Solution was stirred for 15 minutes, and the final product was obtained by evaporation under vacuum. Yield: 70% (2.8mmol). Co(III) for ^{1}H-NMR was prepared by addition of a slight excess of NOBF₄ in acetonitrile and evaporation of the solvent.

^{1}H NMR (400 MHz) CD₃CN, δ (ppm): [Co(ttt)(NCS)₃]: 9.1 (s, 2H); 8.7 (s, 2H); 7.4 (d, 2H); 7.05 (d, 2H); 1.9 (s, 9H); 1.4 (s, 18H). ESI-MS positive **4**: m/z = 242 [TBA]⁺; 518 [Co(ttt)(NCS)]⁺ , m/z calculated for C₂₈H₃₅CoN₄S for 518.19.

2.5 Synthesis of complex 5

Ligand (L³) was sensitized by following a procedure reported in literature [27]. Corresponding Cobalt complex **5** was never reported and was prepared as follows: to 1eq. of ligand L³ (0.5g, 1.2mmol) dissolved in methanol, 1eq. of [Co(H₂O)₆](OTf)₂ (0.84g, 2.4mmol) was added. The resulting solution was stirred for 15 minutes, and the final product was obtained by evaporation under vacuum. **5** was purified by dissolving the solid in a minimum amount of acetonitrile, followed by precipitation with diethyl ether. Yield: 75% (1.4g, 1.8mmol). Co(III) was generated by addition of a slight excess of NOBF₄ in acetonitrile.

^{1}H NMR (400 MHz) CDCl₃, δ (ppm): L³: 9.56 (s, broad, 3H), 8.54 (d, 3H), 8.37 (m, 3H), 7.4 (m, 3H), 3.6 (t, 6H), 3.1 (t, 6H); CD₃CN, δ (ppm): [Co(L³)]³⁺: 8.71 (s, broad, 3H), 8.55 (m, 6H), 7.85 (m, 3H), 7.1 (d, broad, 3H), 3.3 (m, 6H), 2.5 (m, 6H). ESI-MS positive **5**: m/z = 236 [Co(L³)]²⁺, m/z Calculated for C₂₄H₂₇CoN₇: 236.6.

2.6 Synthesis of complexes 6a ,7a

Complex **6a** and **7a** were synthesized as PF₆⁻ salts for comparative purposes (solubility and electrochemical response) according to published reports [24]: the mixing of 1eq. of (NH₄)₂Fe(SO₄)₂ × 6(H₂O) (1g, 2.6 mmol) dissolved in the minimum amount of distilled water with 3eq. of ligand (respectively 2,2'-bipyridine (bpy) (1.2g, 7.8mmol) , 4,4'-dimethyl-2,2'-bipyridine (dmb) (1.45g, 7.8mmol)) afforded the desired compound. Stirring was continued for 15 minutes and complexes **6a** and **7a** were obtained by precipitation with TBAPF₆. All complexes were

purified by dissolving the solid in a minimum amount of acetonitrile, followed by precipitation with diethyl ether and drying at room temperature. Yield **6a**: 86% (1.76g, 2.2mmol); Yield **7a**: 87% (2g, 2.21mmol).

2.7 Synthesis of complexes 6b ,7b

$[Fe(H_2O)_6](OTf)_2$ salt was synthesized by adding to 1eq. of $(NH_4)_2Fe(SO_4)_2 \times 6(H_2O)$ (1g, 2.6mmol) dissolved in the minimum amount of distilled water, 2eq. of NaOH (0.2g, 5.1mmol) under N_2 atmosphere. After formation of a white precipitate $(Fe(OH)_2)$, the addition of 2eq. of HOTf (0.45ml, 5.1mmol) led to the formation of $[Fe(H_2O)_6](OTf)_2$ as a pale green solution. Water was evaporated under vacuum and the solid was dissolved in methanol. Complexes **6b** and **7b** were obtained by adapting the procedure reported at *2.6*, mixing $[Fe(H_2O)_6](OTf)_2$ with 3eq. of ligand (respectively 2,2'-bipyridine (bpy) (1.2g, 7.7mmol), 4,4'-dimethyl-2.2'-bipyridine (dmb) (1.41g, 7.7mmol)). Solution was stirred for 15 minutes, and the final product was obtained by evaporation under vacuum. All complexes were purified by dissolving the solid in a minimum amount of acetonitrile, followed by precipitation with diethyl ether and drying at room temperature. Yield **6b**: 75% (1.57g, 1.9mmol); Yield **7b**: 74% (1.71g, 1.88mmol).

^{1}H NMR (400 MHz) CD$_3$OD ,δ (ppm): **6b** : 8.7 (d, broad, 6H), 8.2 (m, 6H), 7.5 (m, 12H); **7b** : 8.57 (s, broad, 6H), 7.25 (m, 12H), 2.6 (s, 18H).

2.8 Synthesis of complexes 7c ,8 and 9

Complex **7c, 8** and **9** were synthesized by adapting the procedure reported at *2.6*: 1eq. of $(NH_4)_2Fe(SO_4)_2 \times 6(H_2O)$ (1g, 2.6mmol) dissolved in the minimum amount of water was mixed in stoichiometric ratio with selected ligand (respectively 3eq. of 4,4'-dimethyl-2,2'-bipyridine (dmb) (1.41g, 7.7mmol), 3 eq. of 4,4'-di-*tert*-butyl-2,2'-bipyridine (dtb) (2.05g, 7.7mmol) and 2eq. of 4,4',4''-tri-*tert*-butil-2,2':6',2''-terpyridine (ttt) (3.07g, 7.7mmol)). Stirring was continued for 15 minutes, and complexes **7c**, **8** and **9** were obtained by precipitation with LiTFSI (2.2g, 7.7mmol). All complexes were purified by dissolving the solid in a minimum amount of acetonitrile, followed by precipitation with diethyl ether and drying at room temperature. Yield **7c**: 82% (2.03g, 2.1mmol); Yield **8**: 80% (2.49g, 2mmol): Yield **9**: 78% (2.48g, 1.98mmol).

^{1}H NMR (400 MHz) CD$_3$OD ,δ (ppm): **7c** : 8.58 (s, broad, 6H), 7.28 (m, 12H), 2.55 (s, 18H); **8**: 8.68 (s, broad, 6H), 7.58 (dd, 6 H), 7.27 (d, 6 H), 1.48 (s, 54 H); **9**: 9.2 (s, 4H), 8.8 (s, 4H), 7.27 (d, 4H), 6.9 (d, 4H), 1.9 (s, 18H), 1.3 (s, 36 H).

2.8 Synthesis of 6ox

6ox ([Fe(bpy)$_3$](TFSI)$_3$) was synthesized by adding to 1 eq. of **6b** in acetonitrile, an excess of CAN (2eq). The white precipitate ([Fe(bpy)$_3$](NO$_3$)$_3$) was centrifuged and washed several times in acetonitrile. Once dissolved the solid in water, **6ox** was precipitated with an excess of LiTFSI (4eq), as TFSI salt.

3. Results and Discussion

3.1 Structural Characterization

Redox species were obtained with high yields, typically ranging from 70 to 90 % with a good purity which was confirmed by proton NMR. Their identity, which was not ambiguous based on an NMR, showing the expected proton resonances with the appropriate multiplicities, was further confirmed by ESI mass spectrometry on the newest species (**5** and **4**) . A further confirmation of the chemical purity of the samples came from the electrochemical study (see section 3.2), which revealed the presence of a clean voltammetric response, with no different waves other than those expected upon interception of the redox states of these couples. In the case of tri-substituted bipyridine complexes **1**,**2**,**3**,**6a**,**7**a,**6b**,**7b**,**7c**, and **8** , the IR recorded in diffuse reflectance mode in KBr was essentially dominated by the normal modes of the bipyridine (involving mainly C=C and C=N bonds), showing intense absorption in the region ranging from 1600 to 1400 cm^{-1} and by other lower frequency bipyridine skeletal modes at 840 cm^{-1} bearing the main contribution of the out of plane bending modes of the aromatic hydrogens. Aliphatic and aromatic carbons display stretching modes centered around 3000-2900 cm^{-1}. Triflate counter anions display the most intense IR absorption around 1030 cm^{-1}, possibly overlapping with bipyridine modes, whereas the PF$_6$ responds between 820 and 790 cm^{-1}. TFSI anions are characterized by absorption bands which are quite close to those of triflate (ca. 1070 and 1030 cm^1) being dominated by the deformation modes of the CF$_3$ groups. Other lower frequency collective modes involving the SO$_3$ groups are difficult to distinguish due to the proximity of the bending modes of the polypyiridines. **4** shows the characteristic NCS stretching at 2062 cm^{-1}, followed by the normal modes of the terpyridine similar to those of the bipyridines, which are also found for the bis-terpyridine complex **9**. The chelate complex 5, does not show strongly diagnostic peaks, compared to the previous cases considering that the exacoordinated ligand bears both aliphatic and aromatic carbons, nitrogens and hydrogens.

3.2 Electrochemical Characterization in a static three electrode cell.

Half-wave redox potentials (E$_{1/2}$) referred to saturated calomel electrode (SCE) related to Fe(III)/Fe(II) and Co(II)/Co(I) redox couples, measured through cyclic voltammetry in EC:PC + 0.1M LiOTf, are reported in Table 1. Nearly identical E$_{1/2}$ were observed in PC, AcN and AcN:PC

as representative solvents chosen for their electrochemical stability window suitable for their use in redox flow batteries. Cyclic voltammograms of all complexes at glassy carbon (GC) working electrode (WE) show *quasi-reversible* processes associated to metal-ligand centered oxidation and reduction, with peak separation (ΔE (Epa-Epc)) in the range of 0.1 - 0.13 V. Cobalt complexes CVs are characterized by a redox wave corresponding to the reduction of Co(II) to Co(I), with $E_{1/2}$ in the range of -0.98 - -1.16 V vs SCE. The most negative $E_{1/2}$ is observed for **3**, probably due to the electron donating effect of the alkyl substituents. **2** displays a nearly identical $E_{1/2}$, consistent with the similar inductive effect of methyl vs. *tert*-butyl groups. CVs of the iron complexes are characterized by a monoelectronic redox wave corresponding to the oxidation of Fe(II) to Fe(III), with $E_{1/2}$ in the range of 0.8 - 1 V vs SCE. From data reported in Table 1 it is clear that processes related to Co(II)/(I) and Fe(III)/Fe(II) species are energetically suitable to develop potential differences between 1.6V and 2V, if coupled in a redox cell (Fig.4). The highest thermodynamic potential of the charged cell would be expected by coupling **6b** and **3** reaching values close to 2.2 V.

Table 1-Electrochemical parameters extracted from CVs of 10^{-2} M Cobalt and Iron complexes in EC:PC + 0.1M LiOTf

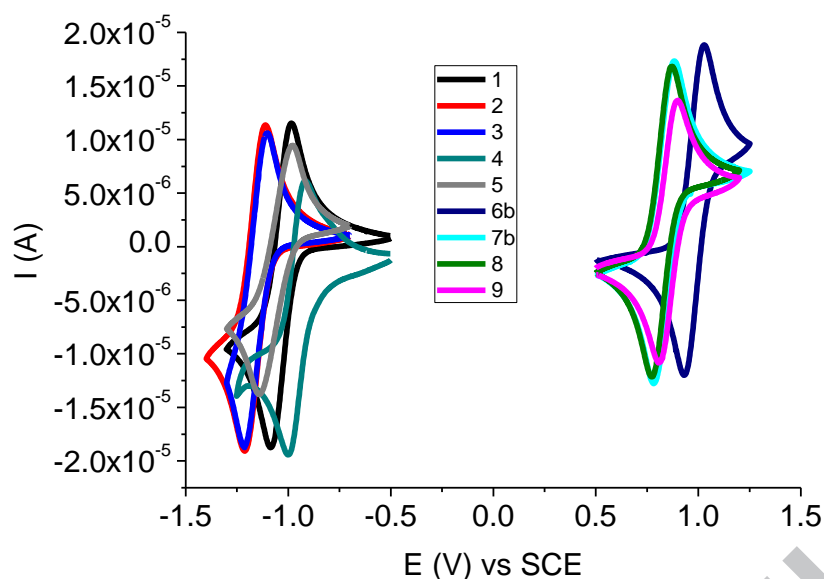|	Co(II)/Co(I)			
	$E_{pa}(V)$	$E_{pc}(V)$	$E_{1/2}(V)$	$\Delta E(V)$
1	-1.07	-0.97	-1.02	0.1
2	-1.2	-1.1	-1.15	0.1
3	-1.21	-1.1	-1.16	0.11
4	-0.93	-1.03	-0.98	0.1
5	-1.13	-1.01	-1.07	0.13
	Fe(III)/Fe(II)			
	$E_{pa}(V)$	$E_{pc}(V)$	$E_{1/2}(V)$	$\Delta E(V)$
6b	0.93	1.03	0.98	0.1
7b	0,.88	0.78	0.83	0.1
8	0.87	0.77	0.82	0.1
9	0.91	0.81	0.86	0.1

11

Fig.4-Cyclic voltammograms of 10^{-2}M Cobalt and Iron complexes in EC:PC + 0.1M LiOTf (scan rate: 10mV/s).

Preliminary stability tests intended to screen the reproducibility of the electrochemical response of the selected series at carbonaceous interfaces, were carried out by recording multiple cycles (100 scans) within -0.2/-1.3 V vs SCE for Co(II)/(I) and within 0.2/1.2 V vs SCE for Fe(III)/(II), at a GC WE. In order to stress electrochemical stability, we have selected high concentrations (10^{-2}M) and slow scan rates (10mV/s), which are more sensitive to adsorbate formation on the electrode surface. In general we have monitored the anodic peak current (Ipa) as an indication of the stability of the electrodic response upon subsequent scans. It can be appreciated, due to a continuous decrease of the peak current upon multiple cycles, that in AcN and AcN:PC cobalt complexes lead to electrode passivation, even when decreasing by an order of magnitude complex concentration (10^{-3}M) (Fig.5 a, b). However, in PC and EC:PC **1**, **2** and **4** show a substantially stable current, which indicates that the electrode surface does not reduce its electroactivity due to formation of adsorbates or electrostatic assemblies between the negatively charged surface and positively charged complexes (Fig.5 c, d) which lead otherwise to the blockage of the electron transfer. It can be also appreciated that complex **4** displays the most stable current up to 100 scans, consistent with the negative charge (varying between 2^{-} (Co(I)) and 1^{-} (Co(II))) which helps to avoid, through electrostatic repulsion, the formation of electrode adsorbates (Fig.5 c, d cyan line). It should be noted that the origin of the electrode passivation should not be related to an intrinsic chemical instability of the cobalt(I) complexes, since: i) no new redox waves resulting from possible decomposition products could be observed and ii) a simple cleaning of the electrode surface with alumina paste was able to fully restore the pristine electrochemical response (Fig.S13).

12

Concerning the iron complexes, passivation is not observed in any of the selected solvents in the specified working conditions (Fig.S14).
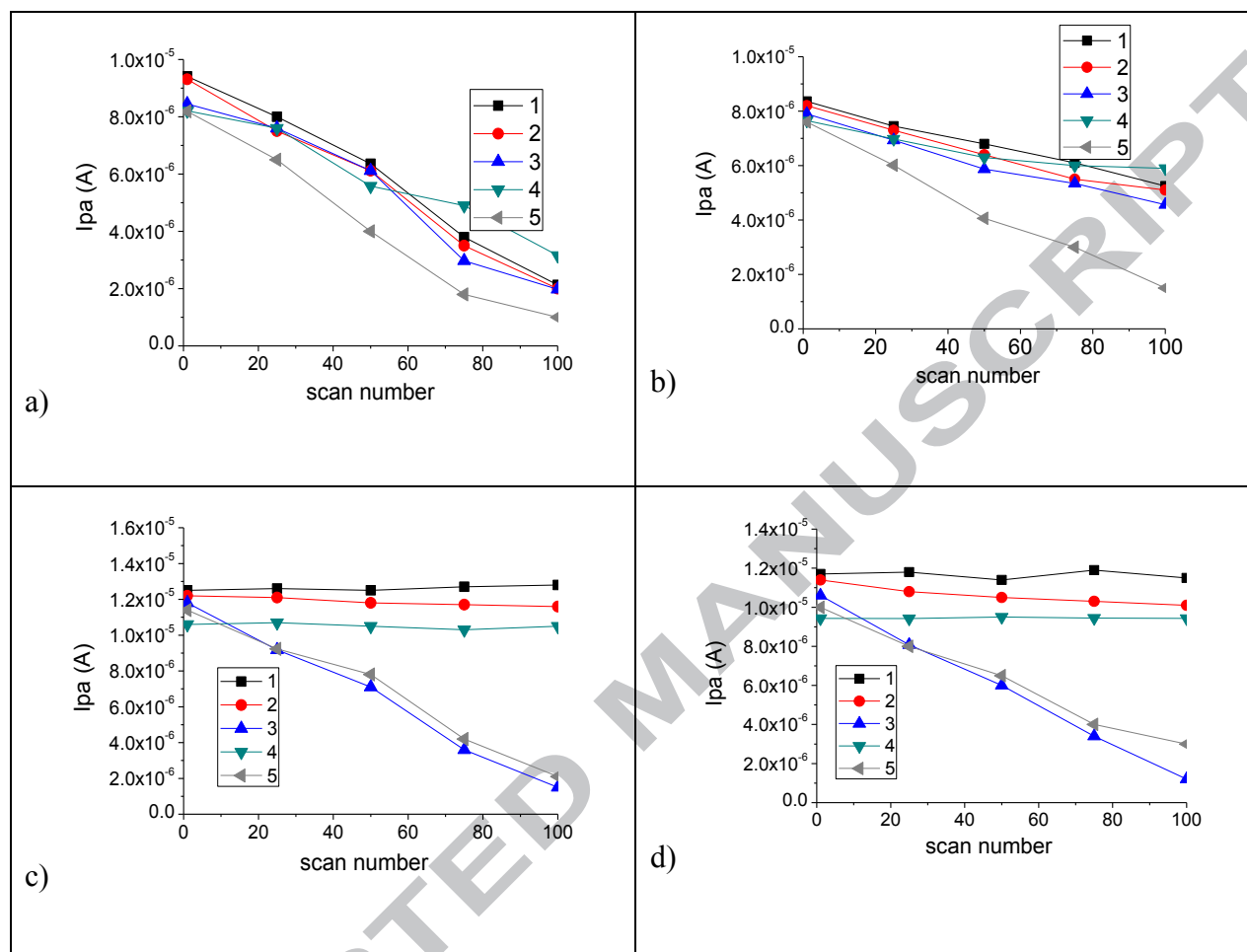

Fig.5- Anodic peak current of cobalt Complexes vs scan number in **a)-**AcN; **b)**-AcN:PC; **c)**-PC; **d)**-EC:PC; + 0.1M LiOTf. In a) and b), cobalt complex concentration is 10^{-3} M (scan rate: 100mV/s). In c) and d) cobalt complex concentration is 10^{-2} M (scan rate: 10 mV/s).

Further stability tests were carried out for Co(II) complexes by employing carbon felt electrodes of the same type of those to be used in flow batteries, polarizing for ca 1h at a potential 300mV more negative than the $E_{1/2}$ of the selected Co(II)/Co(I) couple under stirring. These static electrolysis conditions (i.e. no cycling) are expected to be a severe test for evaluating redox couple stability and formation of secondary species as a result of side reactions accompanying electron transfer. Chronoamperometric tests confirm the generation of a stable current due to Co(I) formation in the case of **1,2** and **4** (Fig.6). On the other hand the cathodic current associated to complexes **3** and **5** decreases with time (Fig.6) which is very evident in the case of **3**, for which the decrease is one-half of the initial value, while **5** displays a much less evident drop during the first hour. Consistent with the preliminary screening at GC WE, CVs recorded after the cathodic polarization do not reveal any response attributable to decomposition byproducts, possibly generated during 1hour long

13

electrolysis: complexes **1**, **2** and **4** (Fig.7 a, b, d) exhibit nearly overlapping voltammetric waves with the initial scan (taken before starting electrolysis). The lack of electrochemically responsive side species is confirmed in the case of complexes **3** and **5** as well (Fig.7 c, e), where the only consequence of the prolonged negative polarization of the carbon felt is a decrease in the intensity of the voltammetric waves with respect to the reference initial scan. In the case of **3**, which displays the least stable response, an increase of the wave separation (ca. 300 mV) is noticed as well, consistent with a decreased electron transfer rate, which confirm the formation of a blocking adsorbate.
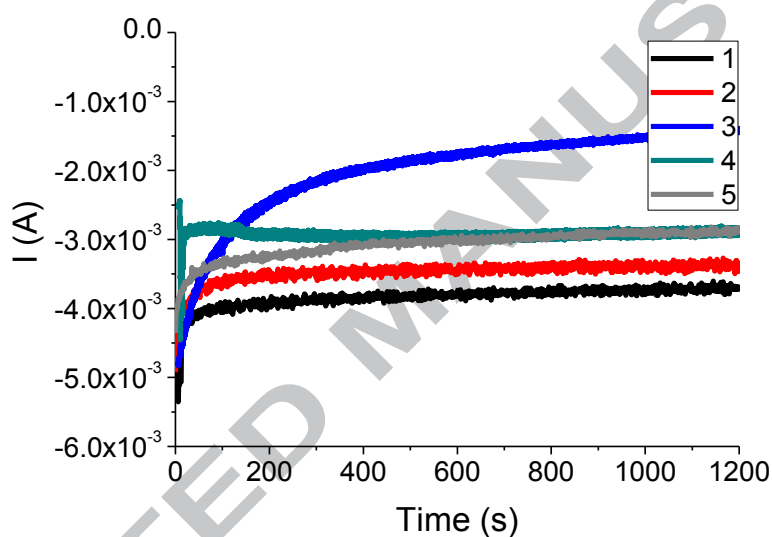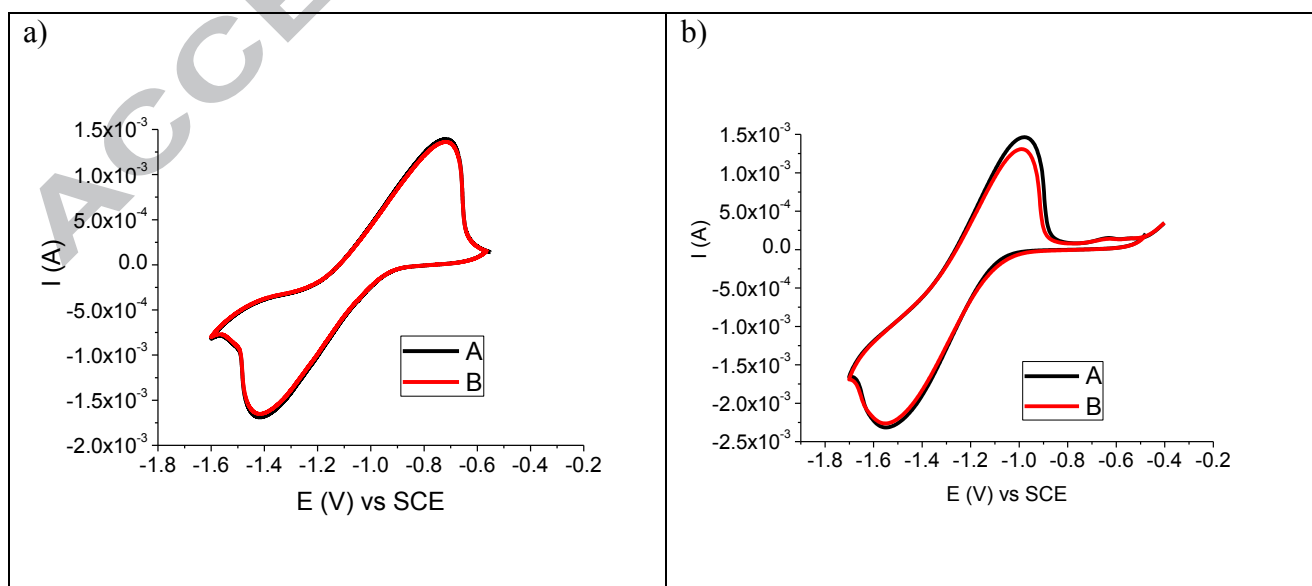

Fig.6- Chronoamperometries of 10^{-2}M Cobalt complexes in EC:PC + 0.1M LiOTf.
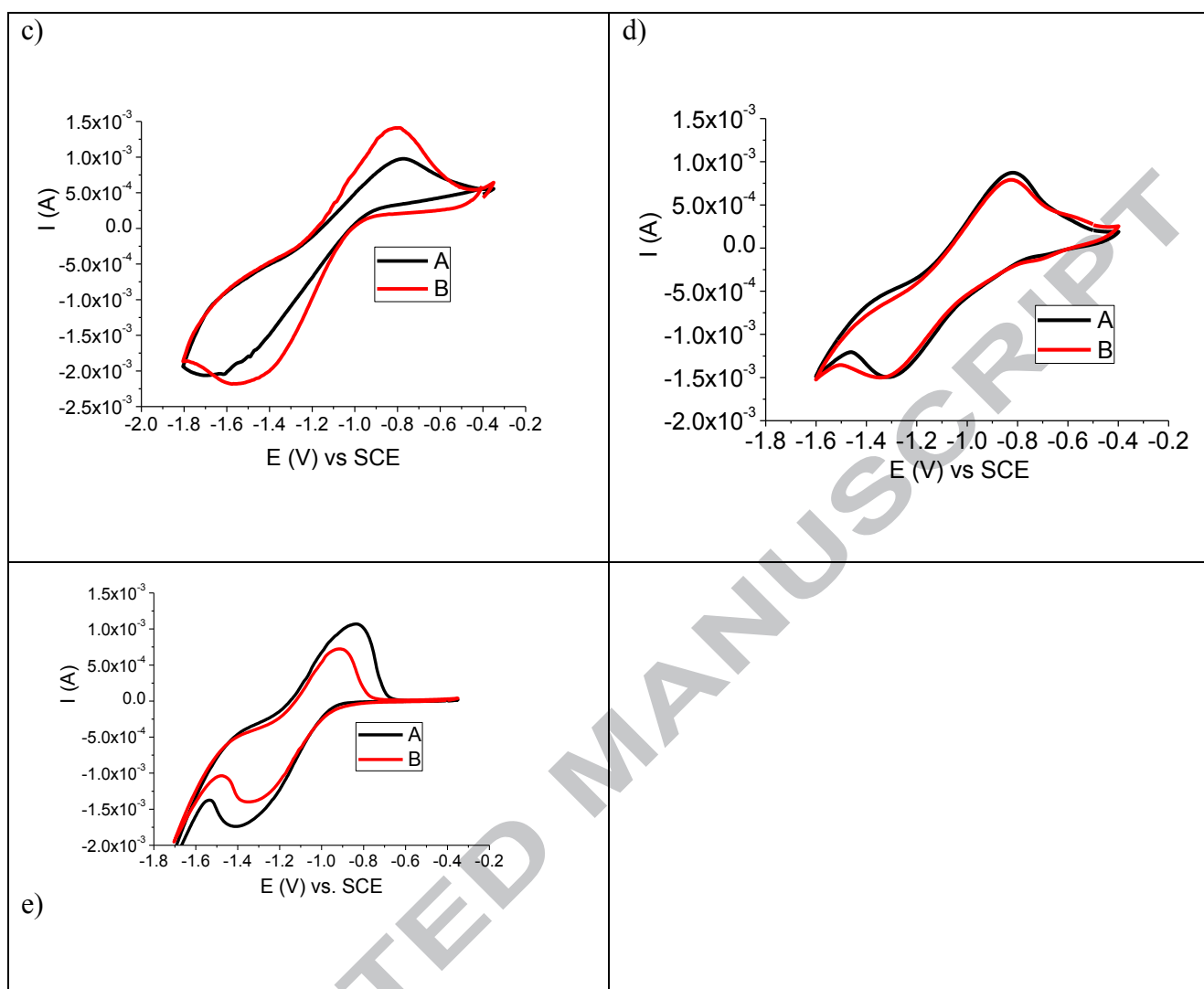
Fig.7- Cyclic Voltammetries of **a**)- **1 b**)- **2 c**)- **3 d**)- **4 e**)- **5** in EC:PC + 0.1M LiOTf at A- t_0 and B- after 1h of cathodic polarization. Cobalt complex concentration is 10^{-2}M.

Kinetic properties of Fe(III)/Fe(II) and Co(II)/Co(I) were investigated by cyclic voltammetry and by electrochemical impedance spectroscopy by employing respectively carbon felt and glassy carbon as working electrodes. The EIS results (Fig.8) at glassy carbon of all complexes at their equilibrium potential could be modeled with a simple circuit comprising the electrochemical interface and the semi-infinite diffusion element. In all cases the charge transfer arc is comparatively small with a charge transfer resistance which is about constant, of the order of 60-70 Ohm. Both in case of iron and cobalt the slowest couples are the *tert*-butyl substituted complexes (i.e. **3**, **8** and **9** bearing the dtb and ttt ligands). **5** also displays not ideal kinetics with respect to the unsubstituted polypyridine ones. The evaluation of its charge transfer properties is however complicated by the limited stability upon prolonged polarization. In all cases the major contribution to the electrode impedance arises

from the diffusional contribution (Wo1-R) which is from 3 to 4 times larger than the charge transfer one. Diffusional resistive contributions of all complexes are comparable (Table 2).
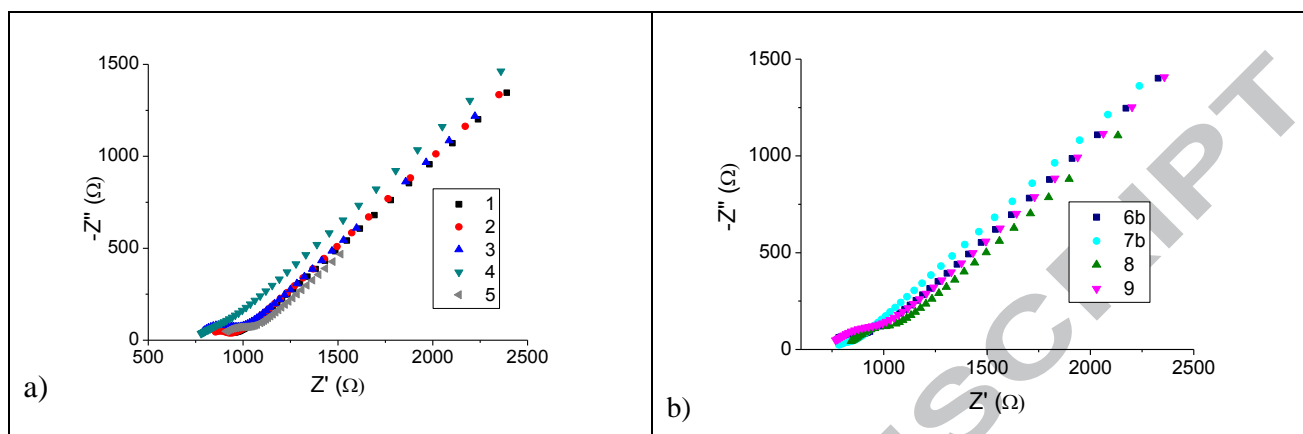

Fig.8 –Nyquist plot of **a**)- 10^{-2}M Cobalt complexes and **b**)- 10^{-2}M Iron complexes in EC:PC + 0.1M LiOTf

Table2 Main resistive contributions in Cobalt and Iron based static three electrode cell.

	Rct	Wo1-R
1	55	356
2	61	371
3	126	389
4	70	384
5	82	408
6b	50	366
7b	57	360
8	97	370
9	80	434

Kinetic properties of Fe(III)/Fe(II) and Co(II)/Co(I) were also screened on carbon felt electrodes. EIS experiments on this type of porous substrates were problematic due to exceeding data dispersion at low frequency and methods based on cyclic voltammetry were implemented in order to extract kinetic and mass transport information. These electrodes have a ratio of active-to-projected area of ca. 50. In general the quasi-reversible behavior of all these redox couples was

16

preserved showing quite similar rate constants within the explored series. The heterogeneous rate constants are of the order of $5\pm1\times10^{-4}$ cm/s (Table 3), leading to equivalent kinetic overpotentials for the two families of iron and cobalt mediators. Diffusion coefficients are also quite comparable, within the experimental error. Values of the order of 8×10^{-7} were commonly found, consistent with the similar structure and coordination environment of these complexes. Thus, mass transport limitations should also be equivalent at the anodic and cathodic compartments of the cell, favoring, in principle, cell balance. These values are about one order of magnitude lower than those found in AcN [28], due to the superior viscosity of the EC:PC mixture. The symmetry factor, extracted from a Butler-Volmer analysis, considering a simple outer sphere electron transfer, are between 0.4 and 0.5, consistent with the symmetric shape of the voltammetric waves.

Table 3- Diffusion coefficients and heterogeneous electron transfer rate constants (k^0) for cobalt and iron complexes.

	$D_{red}(cm^2/s)$	$k^0(cm/s)$	α
1	8.47E-07	6.26E-04	0.45
2	8.07E-07	5.90E-04	0.44
3	7.88E-07	5.13E-04	0.38
4	6.95E-07	4.88E-04	0.4
5	5E-07	4.16E-04	0.4
6b	9E-07	5.34E-04	0.45
7b	8.9E-07	4.64E-04	0.44
8	7.17E-07	4.19E-04	0.38
9	6.9E-07	4.20E-04	0.4

Finally we would like to point out that this study was focused on the triflate salts of complex **6** and **7** (**6b** and **7b**) due to their much higher solubility in EC:PC with respect to the equivalent PF_6 salts, as will be discussed in section *3.3*.

3.3 Solubility

Solubility of most promising complexes in chosen solvents was evaluated to establish the maximum concentrations usable in redox flow batteries at room temperature. Table 4 and Table 5 show results related to iron (II) and cobalt (II) complexes solubility calculated in the selected solvent mixtures.

Table 4 -Cobalt complexes solubility

	PC	EC:PC
1	0.6M	0.68M
2	0.49M	0.53M
3	0.47M	0.5M
4	0.11M	0.15M
5	0.65M	0.7M

Table 5 -Iron complexes solubility

	ACN	AcN:PC	PC	EC:PC
7a	0.2M	0.23M	0.3M	0.32M
7b	0.32M	0.38M	0.46M	0.47M
7c	0.28M	0.3M	0.35M	0.37M
6a	0.24M	0.28M	0.3M	0.35M
6b	0.34M	0.48M	0.56M	0.62M
8	0.3M	0.4M	0.44M	0.46M
9	0.21M	0.25M	0.27M	0.3M

Clearly, complex solubility is affected by the nature of the counter ion, by the nature of peripheric pendants and by the charge of the metal complex, so significant variations of solubility can be expected within this series. The most soluble anodic complexes (Fe (II)) resulted **6b** and **7b** with OTf as counter ion, in EC:PC reaching values close to 0.6 M. The EC:PC has generally better solvent properties than PC alone probably due to higher polarity. TFSI anion also provide satisfactory solubility, but in general it is about 20% lower than the equivalent OTf species. Both TFSI and OTf ensure a much higher solubility than PF_6. A similar trend is found with the cobalt couples, among which **1** reached 0.68 M concentration and **2** 0.5 M concentration in EC:PC. Complex **5,** reaching 0.7 M, was not the one displaying the best response stability at glassy carbon and carbon felt working electrodes and was not considered for the subsequent studies. Unfortunately, the other promising complex **4,** endowed with a good electrochemical stability, reaches only 0.15 M concentration, probably due to its mono-anionic charge leading to less favorable ion-dipole interactions for solvation. The best complexes (**6b** and **1**) with respect to

electrochemical kinetics, stability and solubility will be thus used for further studies approaching application in a real flow battery (see section *3.5*).

3.4 Electronic Absorption Spectroscopy

The absorption characteristics of the redox couple are not of primary importance for cell operation, but the possibility of tracking the charge state of the battery via an independent method, like optical spectroscopy, is a fast method to assess chemical changes occurring during the redox reactions. As far as the optical properties are concerned, Co(II) complexes do not display strong absorption characteristics nor diagnostic fingerprints: electronic absorption spectra of Co(II) complexes, show weak featureless transitions, ostensibly due to population of d-d states at wavelengths > 400 nm, with maximum molar extinction coefficients of ca 700 M^{-1} cm^{-1} (Fig. S17 a). The transitions are only marginally modified by the change in the redox state from Co(II) to Co(I) and from Co(II) to Co(III). By contrast, the electronic absorption spectra of Fe(II) complexes, show MLCT transitions at wavelengths in the range of 500-600 nm, with maximum molar extinction coefficients of ca 10000 M^{-1} cm^{-1}. All spectra are reported in supporting information (Fig.S17 b).

Iron complex **6b** (Fig. S18 a) was chemically reduced and oxidized to explore the possibility of monitoring independently charge and discharge of iron-based cell. Furthermore the storage of the oxidized form of iron for several days without observing chemical decomposition was proved: according to spectrophotometric evidence, Fe(III) **(6ox)** was preserved in EC:PC (Fig.S19) for 30 days, without significant changes during this time. A similar behavior extends to complexes **7b** (Fig. S18 b) and **9** (Fig. S18 c). Chemical reversibility of Iron complex **6b** was confirmed upon electrochemical oxidation-reduction cycles at constant potential in EC:PC. These Cycles were carried out at +1.5V vs SCE, until attainment of a spectrophotometric steady state where the complete bleaching of the MLCT band at 525 nm was observed (Fig.9, red line) whereas the reduced state was regenerated at 0 V showing its complete restoration (blue and black line, overlapping). The reversibility of the iron Fe(II)/(III) **(6b)** was further spectroelectrochemically corroborated by reproducible spectral variations at 525 nm upon fast potential cycling (500 s oxidation at 1.5 V vs SCE and 730 s reduction at 0 V vs SCE) (Fig.S20).
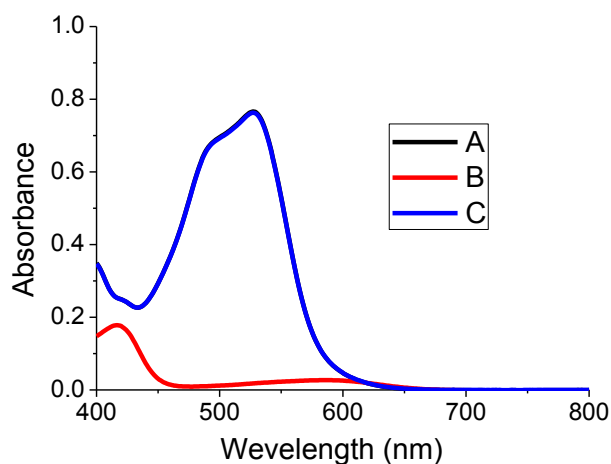
Fig.9- UV-Vis spectra of 10^{-4}M **6b** in EC:PC at A-t_0; B- after 1.5V vs SCE polarization; C- after 0V vs SCE polarization.

3.5 Symmetric thin layer cells

1 and **6b**, the most promising complexes in terms of solubility and electrochemical stability, were examined in a symmetric thin layer cell, to investigate the i-V behavior of these couples in conditions of optimized mass transport, made possible by the use of an inter-electrode spacing of ca. 25 μm, and in concentration of 0.3 M which is relevant to the possible application in the flow battery. EC:PC in the presence of 1 M LiOTf, was the electrolyte of choice for all these studies. In the case of the anodic couple, PEDOT was selected for its generally good electroactivity and for its ease of electrodeposition to yield mechanically stable thin films. The resulting J-V curve is shown in Fig.10a where it can be appreciated the limiting current density of ca. 30 mA/cm^2, the maximum current that can be extrapolated in these working conditions. The diffusion coefficient D, evaluated from limiting current J_L, expressed as $J_L = (2nFCD)/L$, where L is the thickness of the spacer and C is the concentration of the redox couple, results of ca. 1×10^{-6} cm^{2}s^{-1} and is in perfect agreement with the one evaluated from cyclic voltammetry tests (see Section *3.1*). EIS provides deeper insights of the overall electrochemical process, by resolving charge transfer and mass transfer processes in the frequency domain (Fig.10 b). The total resistance observable is ca 30Ω and it can be appreciated that the Nyquist plot recorded at the equilibrium voltage (0 V) is dominated by the diffusion of the redox couple, while the charge transfer arc is so small to be essentially unobservable under these conditions, confirming the fast electron transfer on PEDOT. This means that even under very small overvoltage (10 mV perturbation) mass transport is the limiting process for this redox couple.
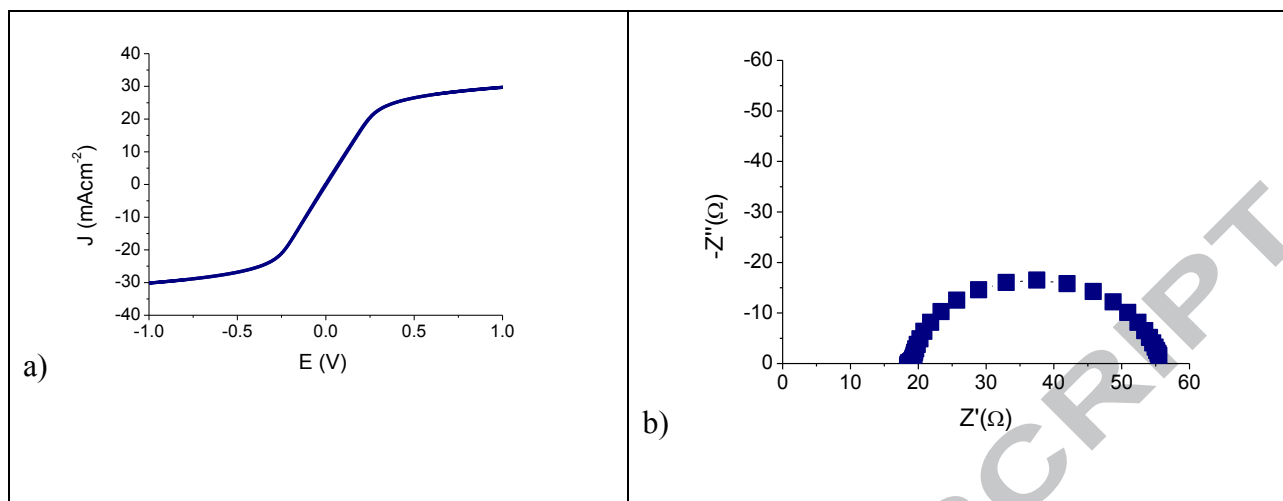
Fig.10 a) – Slow scan rate cyclic voltammetry of 0.3M **6b** in a two-electrode cell in EC:PC + 1M LiOTf **b)** –Nyquist plot of 0.3M **6b** in a two-electrode cell in EC:PC + 1M LiOTf

An analogous preliminary analysis was carried out for **1** by exploring, with CNH cells, the 0.5/-2 V interval in order to screen the entire electrochemical region associated with cobalt redox states: **1** presents waves associated to Co(II)/(I) ($E_{1/2}$ = -1.25 V) and Co(III)/(II) (0 V) processes, in agreement with values observed in cyclic voltammetry. The performance at [Co(II)] = 0.3, where a limiting current density of the order of 25 mA/cm^2 at ca. -1.5 V was observed, matches well the limiting current that could be delivered by Fe(III)/(II) compartment at the selected concentration. Cobalt diffusion coefficient of ca 8 ×10^{-7} cm^{2}s^{-1}, similar to iron, were indeed found, in agreement with the one found in Section *3.1*. No loss in electroactivity nor appearance of electroactive decomposition byproducts were observed after multiple cycling and 24h rest of the cell, confirming the stability of Co(II)/(I) response on carbon substrates even under a concentration suitable for the application in a real cell (Fig.11 a). In 24h there is a slight increase in the total cell resistance, which is, however, attributable to the ohmic resistance, which has a variability of a few ohms (typically 1-5) related to metal / FTO contact. EIS confirm also in this case a dominant role of the diffusion, whose arc is the predominant feature of the Nyquist plot. Consistent with the steep slope of the Co(II)/(I) process, the diffusional arc reaches an amplitude of 30 Ω (Fig.11 b), which perfectly matches with the resistance observed with Fe(III)/(II), thus providing promising expectations for the coupling of these two complexes in liquid battery for energy storage.
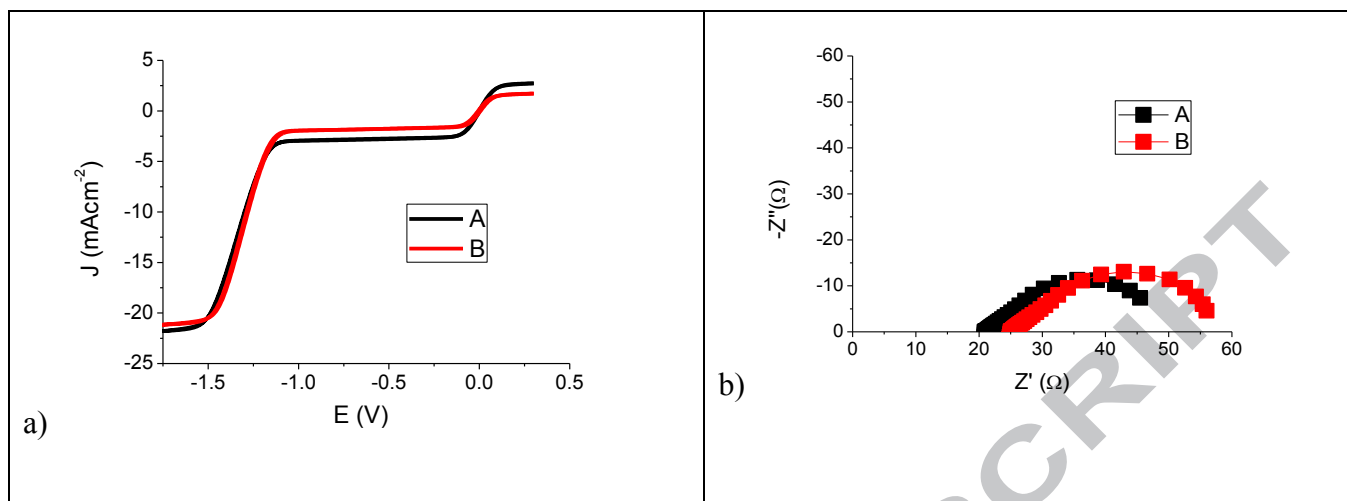
21

Fig.11 a)- Slow scan rate cyclic voltammetry of 0.3M **1** in EC:PC + 1M LiOTf at A- t0 B- after 24h **. b)-**Nyquist plot of 0.3M **1** in EC:PC + 1M LiOTf at A- t_0 B- after 24h.

4. Conclusion

A series of Co(II) and Fe(II) polypyridine complexes as trifilate and TFSI salts were explored with the aim of evaluating their chemical and electrochemical characteristics for application in the framework of redox flow batteries. Among the explored series the best results were observed with complexes **6b** and **1** which couple solubility > 0.6 M in EC:PC and chemical stability upon slow rate potential cycling and potentiostatic electrolysis with diffusion limited electron transfer processes. The exploitation of Co(II)/(I) and Fe(II)/(III) states allows to obtain open circuit voltages close to 2 V, with the delivery of limiting current of the order of 30 mA/cm^2 when the mass transport conditions are optimized. The use of iron complexes with strongly colored MLCT states offer in addition the possibility of monitoring the charge state of the battery via fast optical methods. The same methods are less successful with cobalt which is endowed with low extinction coefficients in the visible. Given these promising properties selected iron and cobalt couples are under testing in lab scale organic redox flow batteries for efficiency and stability evaluations.

Acknowledgments

5.References

[1] Q. Huang, Q. Wang, Next-Generation, High-Energy-Density Redox Flow Batteries, ChemPlusChem, 80 (2015) 312-322.

[2] G. Kear, A.A. Shah, F.C. Walsh, Development of the all-vanadium redox flow battery for energy storage: a review of technological, financial and policy aspects, International Journal of Energy Research, 36 (2012) 1105-1120.

[3] J.S.J. E. Wesoff, Largest capacity Flow Battery in North America and EU is on-line and commissioned, in, 2015.

[4] M. Miller, A. Bourke, N. Quill, J. Wainright, R. Lynch, D. Buckley, R. Savinell, Kinetic study of electrochemical treatment of carbon fiber microelectrodes leading to in situ enhancement of vanadium flow battery efficiency, Journal of The Electrochemical Society, 163 (2016) A2095-A2102.

[5] F. Rahman, M. Skyllas-Kazacos, Vanadium redox battery: Positive half-cell electrolyte studies, Journal of Power Sources, 189 (2009) 1212-1219.

[6] P. Leung, X. Li, C.P. De León, L. Berlouis, C.J. Low, F.C. Walsh, Progress in redox flow batteries, remaining challenges and their applications in energy storage, Rsc Advances, 2 (2012) 10125-10156.

[7] S. Eckroad, Vanadium redox flow batteries: an in-depth analysis, Electric Power Research Institute, Palo Alto, CA, 1014836 (2007).

[8] Y. Huang, S. Gu, Y. Yan, S.F.Y. Li, Nonaqueous redox-flow batteries: features, challenges, and prospects, Current Opinion in Chemical Engineering, 8 (2015) 105-113.

[9] A.E. Sleightholme, A.A. Shinkle, Q. Liu, Y. Li, C.W. Monroe, L.T. Thompson, Non-aqueous manganese acetylacetonate electrolyte for redox flow batteries, Journal of Power Sources, 196 (2011) 5742-5745.

[10] J. Mun, M.-J. Lee, J.-W. Park, D.-J. Oh, D.-Y. Lee, S.-G. Doo, Non-aqueous redox flow batteries with nickel and iron tris (2, 2'-bipyridine) complex electrolyte, Electrochemical and Solid-State Letters, 15 (2012) A80-A82.

[11] M.-S. Park, N.-J. Lee, S.-W. Lee, K.J. Kim, D.-J. Oh, Y.-J. Kim, High-Energy Redox-Flow Batteries with Hybrid Metal Foam Electrodes, ACS applied materials & interfaces, 6 (2014) 10729-10735.

[12] Y. Ding, Y. Zhao, Y. Li, J.B. Goodenough, G. Yu, A high-performance all-metallocene-based, non-aqueous redox flow battery, Energy & Environmental Science, 10 (2017) 491-497.

[13] X. Xing, Y. Zhao, Y. Li, A non-aqueous redox flow battery based on tris (1, 10-phenanthroline) complexes of iron (II) and cobalt (II), Journal of Power Sources, 293 (2015) 778-783.

[14] C.G. Armstrong, K.E. Toghill, Cobalt (II) complexes with azole-pyridine type ligands for non-aqueous redox-flow batteries: Tunable electrochemistry via structural modification, Journal of Power Sources, 349 (2017) 121-129.

[15] X. Xing, D. Zhang, Y. Li, A non-aqueous all-cobalt redox flow battery using 1, 10-phenanthrolinecobalt (II) hexafluorophosphate as active species, Journal of Power Sources, 279 (2015) 205-209.

[16] Q. Liu, A.A. Shinkle, Y. Li, C.W. Monroe, L.T. Thompson, A.E. Sleightholme, Non-aqueous chromium acetylacetonate electrolyte for redox flow batteries, Electrochemistry Communications, 12 (2010) 1634-1637.

[17] P.J. Cabrera, X. Yang, J.A. Suttil, R.E. Brooner, L.T. Thompson, M.S. Sanford, Evaluation of tris-bipyridine chromium complexes for flow battery applications: impact of bipyridine ligand structure on solubility and electrochemistry, Inorganic chemistry, 54 (2015) 10214-10223.

[18] Q. Liu, A.E. Sleightholme, A.A. Shinkle, Y. Li, L.T. Thompson, Non-aqueous vanadium acetylacetonate electrolyte for redox flow batteries, Electrochemistry Communications, 11 (2009) 2312-2315.

[19] R.M. Darling, K.G. Gallagher, J.A. Kowalski, S. Ha, F.R. Brushett, Pathways to low-cost electrochemical energy storage: a comparison of aqueous and nonaqueous flow batteries, Energy & Environmental Science, 7 (2014) 3459-3477.

[20] T. Ayers, S. Scott, J. Goins, N. Caylor, D. Hathcock, S.J. Slattery, D.L. Jameson, Redox and spin state control of Co (II) and Fe (II) N-heterocyclic complexes, Inorganica Chimica Acta, 307 (2000) 7-12.

[21] C. Bignozzi, R. Argazzi, R. Boaretto, E. Busatto, S. Carli, F. Ronconi, S. Caramori, The role of transition metal complexes in dye sensitized solar devices, Coordination Chemistry Reviews, 257 (2013) 1472-1492.

[22] S. Carli, E. Busatto, S. Caramori, R. Boaretto, R. Argazzi, C.J. Timpson, C.A. Bignozzi, Comparative evaluation of catalytic counter electrodes for Co (III)/(II) electron shuttles in regenerative photoelectrochemical cells, The Journal of Physical Chemistry C, 117 (2013) 5142-5153.

[23] L. Casarin, W.B. Swords, S. Caramori, C.A. Bignozzi, G.J. Meyer, Rapid Static Sensitizer Regeneration Enabled by Ion Pairing, Inorganic Chemistry, (2017).

[24] S. Cazzanti, S. Caramori, R. Argazzi, C.M. Elliott, C.A. Bignozzi, Efficient non-corrosive electron-transfer mediator mixtures for dye-sensitized solar cells, Journal of the American Chemical Society, 128 (2006) 9996-9997.

[25] F. Ghamouss, R. Pitson, F. Odobel, M. Boujtita, S. Caramori, C.A. Bignozzi, Characterization of screen printed carbon counter electrodes for Co (II)/(III) mediated photoelectrochemical cells, Electrochimica Acta, 55 (2010) 6517-6522.

[26] S. Carli, L. Casarin, Z. Syrgiannis, R. Boaretto, E. Benazzi, S. Caramori, M. Prato, C.A. Bignozzi, Single Walled Carbon Nanohorns as Catalytic Counter Electrodes for Co (III)/(II) Electron Mediators in Dye Sensitized Cells, ACS applied materials & interfaces, 8 (2016) 14604-14612.

[27] S. Mandal, D.K. Seth, P. Gupta, Encapsulating ruthenium and osmium with tris (2-aminoethyl) amine based tripodal ligands, Polyhedron, 31 (2012) 167-175.

[28] J.J. Nelson, T.J. Amick, C.M. Elliott, Mass transport of polypyridyl cobalt complexes in dye-sensitized solar cells with mesoporous TiO2 photoanodes, The Journal of Physical Chemistry C, 112 (2008) 18255-18263.